Available online at www.sciencedirect.com
SCIENCE DIRECT®
PERGAMON
Engineering Applications of Artificial Intelligence 15 (2002) 273–283
Engineering Applications of
ARTIFICIAL
INTELLIGENCE
www.elsevier.com/locate/engappai

Neural network classifiers applied to condition monitoring of a pneumatic process valve actuator

M. Karpenko, N. Sepehri*

Experimental Robotics and Teleoperations Laboratory, Department of Mechanical and Industrial Engineering, The University of Manitoba, Winnipeg, Manitoba, Canada R3T 5V6

Accepted 21 September 2002

Abstract

As modern process plants become more complex, the ability to detect and identify the faulty operation of pneumatic control valves is becoming increasingly important. In this work, a neural network pattern classifier is employed to carry out fault diagnosis and identification upon the actuator of a Fisher–Rosemount 667 industrial process valve. The network is trained with experimental data obtained directly from a software package that comes with the valve. This has eliminated the need for additional instrumentation of the valve. Using this software, tests are carried out to obtain experimental parameters associated with the valve performance for incorrect supply pressure, diaphragm leakage, and vent blockage faults. Specifically, the valve signature and dynamic error band tests are used to directly obtain lower and upper bench sets, minimum, maximum, and average dynamic errors, as well as the dynamic linearity. Additionally, valve deadband and hysteresis are measured graphically from the available valve signature plots for each faulty condition. The relationships between these parameters, for each fault, form signatures that are subsequently learned by a multilayer feedforward network trained by error back-propagation. The test results show that the resulting network has the ability to detect and identify various magnitudes of each fault. It is also observed that a smaller network with a shorter training time results when the valve deadband and hysteresis are included in the training data. Thus, the extra effort required to extract these parameters from the valve signature plots is justified.

Keywords: Condition monitoring; Fault detection and identification; Fault diagnosis; Pneumatic process valves; Neural networks; Pattern classifiers

1. Introduction

Pneumatic control valves are commonly used in modern process plants to control the flow of a fluid, gas or slurry. Failures of these valves give rise to disturbances that result in a non-uniform process output, or if severe, a plant shut down. In either case, the cost of production is increased. Clearly, as process plants become more complex, the need for suitable techniques for detecting both the onset and cause of faulty operations in process valves is becoming increasingly important.

In general, fault detection and identification (FDI) schemes are designed to diagnose the faulty operation of a dynamic system by monitoring some aspects of the system's performance, such as a critical temperature or pressure. Then, when it is evident that a fault has occurred (fault detection), a decision is made as to the cause of the fault (fault identification). The most popular of the modern FDI techniques is the model-based approach (Frank, 1990). Here, a priori mathematical information is used to model the normal system. Based upon the system model, state or parameter estimation techniques are then used to facilitate a comparison between the actual process and the modelled process to accomplish fault detection. This comparison can also be used to generate a vector of residuals from which the cause of the fault may be identified by a knowledge-based, statistical or geometric method (Isermann, 1997; Leonhardt and Ayoubi, 1997). One weakness of the model-based techniques is that they are generally restricted to linear systems or nonlinear systems that have been linearised about some operating point. Furthermore, in cases where only a poor or

*Corresponding author. Tel.: +1-204-474-9804; fax: +1-204-275-7507.
E-mail address: nariman@cc.umanitoba.ca (N. Sepehri).

0952-1976/02/$ - see front matter © 2002 Elsevier Science Ltd. All rights reserved.
PII: S0952-1976(02)00068-4

imprecise analytical model is available, the model-based approach to FDI is problematic (Frank, 1990). With respect to the pneumatic process control valve studied here, developing an analytical model is complicated due to the nonlinear characteristics of the nozzle-flapper (Burrows and Peckham, 1977), pneumatic relay and coulomb friction between the valve stem and valve body. Furthermore, the analytical model requires simultaneous consideration of the laws of thermodynamics, compressible fluid dynamics, as well as Newtonian mechanics (French and Cox, 1990). To overcome the limitations of the model-based approach, some researchers have used neural networks to generate the models (Borairi and Wang, 1998; Bernieri et al., 1994). Particularly, McGhee et al. (1997) used multilayer feedforward networks to model the output torque of a rotary-type valve. While their approach can certainly be used to detect faulty operation of the valve, it cannot be used to determine the cause of the fault since only one dynamic parameter is available for analysis.

Neural networks can also be used in a different way to solve the FDI problem. In contrast to being used to generate system models, neural networks can be implemented as pattern classifiers. In the latter case, sets of parameters that contain information about the operating condition of the dynamic system under consideration are first obtained for normal operation as well as for a number of faulty operating conditions. If carefully selected, these parameter sets will contain not only information about the presence of a fault, but also information that can be used to identify the cause of the fault. The specific values of each parameter in the sets are akin to fingerprints in the sense that they identify the particular faulty condition and its relative magnitude. These fault signatures are then learned by a neural network classifier through a training process. Using neural networks to solve the FDI problem in this way is attractive due to the ability of neural networks to learn the relationships between the fault signatures and the corresponding operating conditions of the system (Tzafestas and Dalianis, 1994). Furthermore, neural networks eliminate the need for establishing the heuristic rules that are required in the knowledge-based approaches to FDI. For examples of the knowledge-based approach see Frank (1990), Isermann (1993) as well as Sharif and Grosvenor (2000). Moreover, if the parameters that make up the fault signatures can be obtained directly from available data, the development of a system model is not required. This further simplifies the FDI system.

The fundamental requirement for successful implementation of the pattern classifier technique for FDI is the availability of a relevant, information rich, set of input data for each of the faults in question. Selecting such a data set from a seemingly infinite pool of information is a difficult task. However, it is often the case that useful information can be obtained from the available data through feature extraction (Bishop, 1995). Conceptually, the idea of feature extraction is to find those parameters that give the most information about the condition of the system and discard the rest.

A number of different approaches have been taken to solve the feature extraction problem for pattern-classification-based FDI. One is to use discrete measurements of the system states as the inputs to the neural network. Here, the assumption is made that the relationship between each of the measured states changes in a characteristic way, in the presence of each fault. Le et al. (1997) and Crowther et al. (1998) have used this approach towards FDI of fluid power systems. A more elaborate approach was taken by Le et al. (1998) where linear prediction coding was used to generate inputs to the neural network classifier. Other researchers (Yen and Lin, 2000; Lin and Qu, 2000; Zhang et al., 2000) have shown that wavelet transforms are also powerful tools for feature extraction. It should be noted, however, that in order to apply any of the above methods, considerable instrumentation of the system is generally required. Such a proposition could be expensive, time consuming, and in some instances may not even be possible without substantial modification of the existing equipment.

In the case of the valve studied here, the manufacturer has developed the ValveLink™ software package (Fisher Controls Inc., 1999a). The software allows users to directly measure a number of performance parameters associated with the operation of the valve. The intent is to aid maintenance personnel in assessing the condition of the valve, based on the measured values. However, specialist knowledge is often required for the identification of faulty operation from the data obtained via the software (Karpenko et al., 2001). Moreover, some faults are prone to misinterpretation even by the specialists (Sharif and Grosvenor, 2000). This has motivated the present investigation into an automated approach towards FDI of the process valves.

The goal of this work is to design a FDI scheme based upon a neural network pattern classifier to detect and identify actuator faults for a Fisher-Rosemount 667 control valve. The ValveLink™ software is used as a feature extraction device to measure several parameters, indicative of the valve condition. This is desirable since the data are readily available and no additional instrumentation of the valve is necessary. Using the software, performance parameters related to the valve signature and the dynamic error band (DEB) tests are obtained and are used as network inputs. The valve signature test generates four parameters. The lower and upper bench sets, indicative of the pressure range over which motion of the valve stem occurs, are acquired automatically by the software. The valve deadband and

hysteresis are obtained graphically from the corresponding valve signature plots. The DEB test automatically generates four parameters associated with the relationship between the valve position and the control signal. These are the minimum, maximum, and average dynamic errors, and the dynamic linearity. The eight parameters associated with the performance tests are determined experimentally for a number of faulty operating conditions. The faults of interest are various levels of incorrect supply pressure, diaphragm leakage and actuator vent blockage. These faults are commonly found in industrial settings (McGhee et al., 1997; Sharif and Grosvenor, 1998; Karpenko et al., 2001). Using the available data, a multilayer feedforward network is then trained by error back-propagation to detect and identify various magnitudes of the faults of interest. The multilayer feedforward network structure has been shown to perform well for a number of pattern-classification-based FDI problems (Sorsa et al., 1991; Koivo, 1994; Le et al., 1997, 1998; Crowther et al., 1998; Karpenko et al., 2001; Karpenko and Sepehri, 2001).

In the next section, the experimental system is described. The modifications to the valve allowing the faults to be introduced to the system are also explained. Then, the valve signature and DEB tests and the associated performance parameters are defined. Next, the FDI scheme is developed and the structure of the neural network classifier is discussed along with some considerations regarding its training. Finally, the performance of the FDI scheme is assessed. This is followed by some concluding remarks.

2. Experimental system

2.1. Pneumatic control valve

The control valve used in this work is shown in Fig. 1. It is a Fisher–Rosemount 667, retrofitted so that the various faults of interest could be experimentally introduced in the system. The valve consists of three main components: (i) the flow control device or valve body, (ii) the pneumatically driven diaphragm-type actuator, and (iii) the digital valve controller (DVC) that closes the loop.

The DVC module consists of a printed circuit board, a current to pressure (I/P) converter, and a pneumatic relay. The I/P converter, is a field-controlled nozzle-flapper arrangement that causes the opening or closing of the pneumatic relay, thus generating a control pressure. With reference to Fig. 2, the control pressure generated by the DVC is supplied to the lower chamber of the actuator. The resulting force unbalance across the diaphragm causes the valve to open or close.

In addition to the control electronics, the DVC contains a potentiometer-type position sensor to measure the position of the valve stem and a pressure transducer to monitor the lower chamber pressure. The onboard sensors of the DVC are able to communicate with the ValveLink™ software via a standard RS-232 interface (Fisher Controls Inc., 1999a).

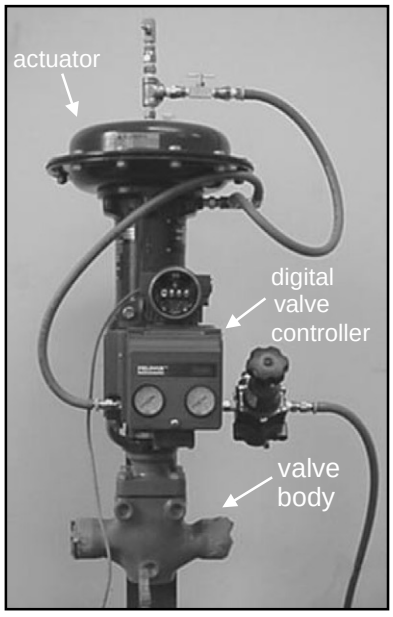

Fig. 1. Fisher–Rosemount 667 pneumatic process valve.

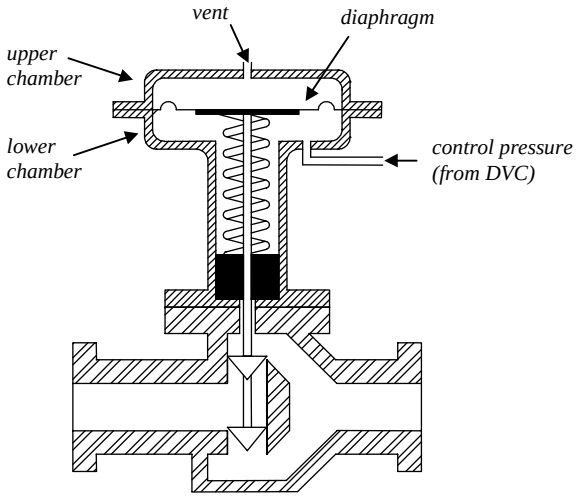

Fig. 2. Cross-sectional view of actuator and valve body.

2.2. Faulty operating conditions

The incorrect supply pressure fault may arise either as the result of blockages or restrictions in the air supply lines or due to increased demand placed on the plant air supply. The supply pressure directly influences the amount of air that can be delivered to the lower actuator chamber by the DVC. Consequently, the transient response of the valve can be severely affected

by this fault (Fisher Controls Inc., 1999b). To create the incorrect supply pressure fault in the experimental test rig, a pressure regulator was installed between the plant air supply and the DVC as shown in Fig. 3.

The purpose of the actuator vent is to purge air from the upper actuator chamber when the valve is opened and to allow air into the upper chamber when the valve is closed. When the valve opens suddenly and the actuator vent is blocked, pneumatic pressure builds in the upper chamber. This pressure surge increases the damping and impairs the system performance. Similarly, if the valve is suddenly closed and the vent is blocked, a partial vacuum is created in the upper chamber. Again, the damping is increased and the system performance is diminished. In order to simulate this fault, an adjustable needle valve was inserted into the vent port as illustrated in Fig. 3. The full-open and full-closed positions of the needle valve were designated as 0% and 100% vent blockage, respectively.

As the valve is actuated, the flexible diaphragm is subjected to cyclic stresses. Thus, the diaphragm is especially prone to fatigue failure that initially manifests itself as localised defects in the diaphragm material. These defects cause the leakage of air across the diaphragm. If this leakage is not detected, the diaphragm will eventually rupture and render the valve useless. Hence, it is important to detect diaphragm leakages as they develop. As shown in Fig. 3, the diaphragm leakage was simulated by bypassing air from the lower chamber to the upper chamber by means of a flexible hose. The airflow was controlled by an adjustable needle valve. The position of the needle valve where the control valve ceased to respond to any input signal was denoted as 100% diaphragm leakage, or total diaphragm failure.

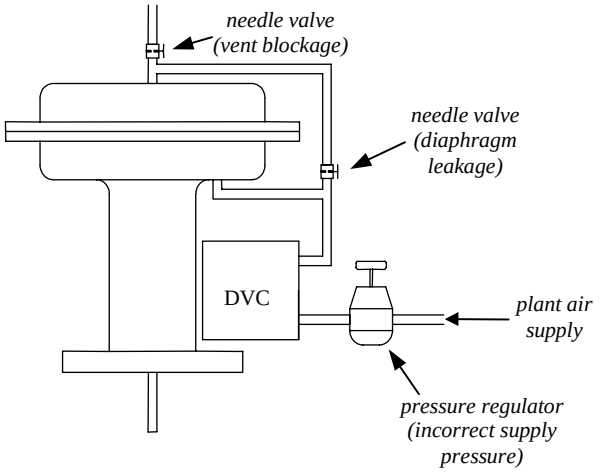

Fig. 3. Schematic of the experimental set-up illustrating the methods by which various faults were introduced into the system. The pressure regulator allows incorrect supply pressures to be set while the two needle valves allow diaphragm leakage and vent blockage faults to be simulated.

3. Valve performance tests

The ValveLink™ software was used to carry out the valve signature and the DEB tests for a number of faulty operating conditions that were simulated experimentally. These tests and performance parameters they generate are outlined next.

3.1. Valve signature test

The valve signature test monitors the position of the valve stem as the pressure in the lower actuator chamber is cycled between atmospheric and the full supply pressure. A typical valve signature plot for a healthy valve is shown in Fig. 4. As illustrated, the pressure-position profile is loop-like, with one curve followed as the valve is opened (opening trace) and the other as the valve is closed (closing trace). The loop-like profile is a result of the friction between the valve stem and the valve stem packing. The shape of the loop is influenced by faulty operation of the valve. This is illustrated in Fig. 5, which shows valve signatures for various faults along with the signature of the healthy valve.

Two performance parameters associated with the valve signature plot are calculated automatically. With reference to Fig. 4, they are: (i) *lower bench set*—the average pneumatic pressure at which the valve meets the lower actuator stop, and (ii) *upper bench set*—the average pneumatic pressure at which the valve meets the upper actuator stop. Two additional parameters, illustrated in Fig. 4, that are easily measured from the valve signature plot are: (i) *deadband*—the range through which the lower chamber pressure can be varied without a noticeable change in the displacement of the valve, when the direction of motion is reversed, and (ii) *hysteresis*—the maximum difference in the

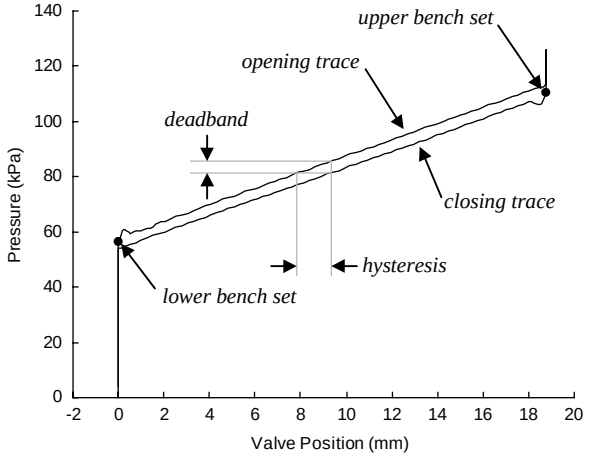

Fig. 4. Typical valve signature plot for a healthy valve illustrating the lower and upper bench sets, as well as the valve deadband and hysteresis.

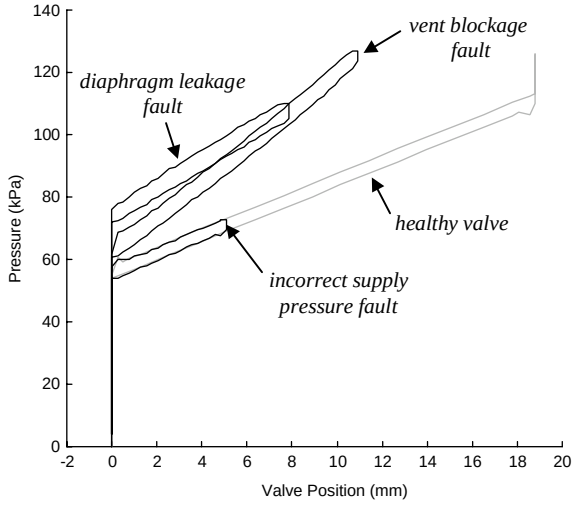

Fig. 5. Valve signature plots corresponding to various failure modes. The signature of a healthy valve is included for reference.

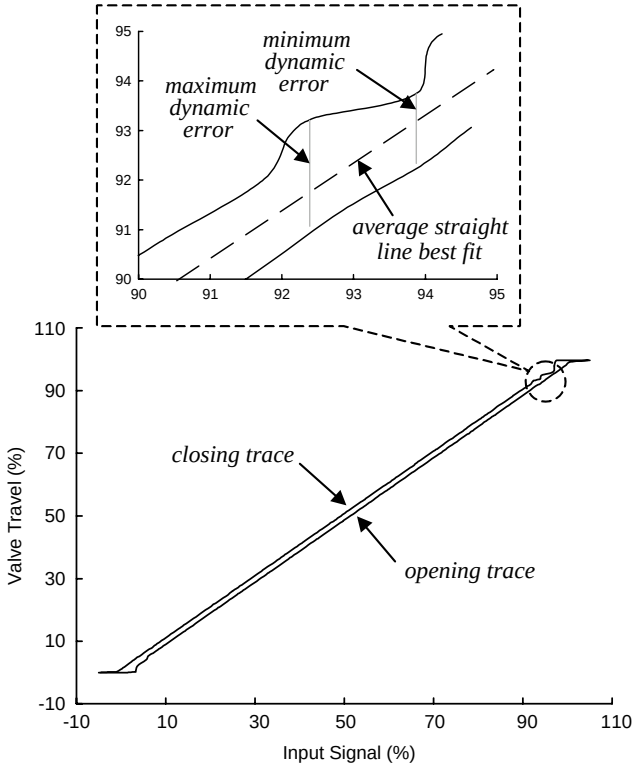

Fig. 6. Typical dynamic error band plot for a healthy valve. The minimum and maximum dynamic errors are defined and the straight line best fit to the average of the opening and closing cures is shown.

position of the valve stem for a given lower chamber pressure, when the direction of motion is reversed.

3.2. DEB test

The DEB test establishes the relationship between the valve position and the control signal as the latter is

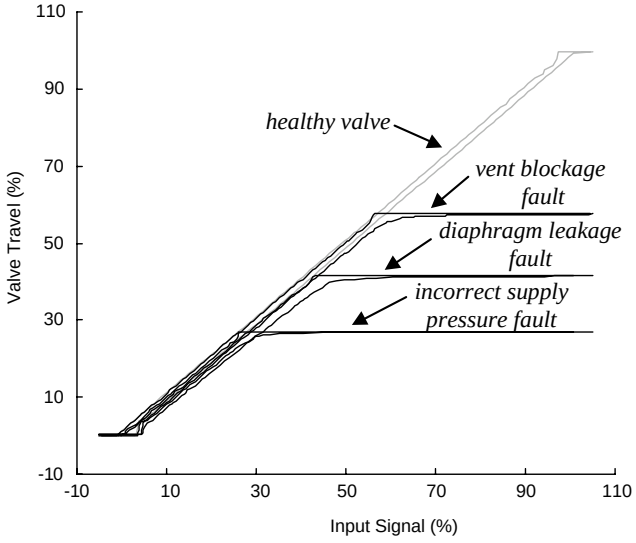

Fig. 7. Dynamic error band plots corresponding to various failure modes. The trace for a healthy valve is included for reference.

varied from −5% to 105% of its normal operating range. A typical DEB plot for a healthy valve is shown in Fig. 6. As in the case of the valve signature plot, the loop-like profile is the result of the friction between the valve stem and the valve stem packing. The shape of the loop is influenced by faulty operation of the valve. This is shown in Fig. 7, which compares the DEB plots for various faults with that of the healthy valve. As is seen, the faults also keep the valve from achieving its full range of motion.

Referring to Fig. 6, four parameters associated with the DEB test that are calculated automatically by the software. They are: (i) *minimum dynamic error*—the minimum distance between the opening and closing traces, (ii) *maximum dynamic error*—the maximum distance between the opening and closing traces, (iii) *average dynamic error*—the mean of the minimum and maximum dynamic errors, and (iv) *dynamic linearity*—the maximum deviation between the straight line best fits to each of the opening and closing traces and a straight line best fit to the average value of the traces.

4. Fault detection and identification scheme

The proposed FDI scheme is illustrated in Fig. 8. The FDI procedure involves two stages. The first is the measurement of the valve performance parameters via the valve signature and DEB tests. The particular values of the performance parameters form a fault signature, which is then passed to the neural network for classification. The neural network estimates the operating condition of the valve in terms of the supply pressure, percent vent blockage and percent diaphragm leakage. Thus, the occurrence of a specific fault is

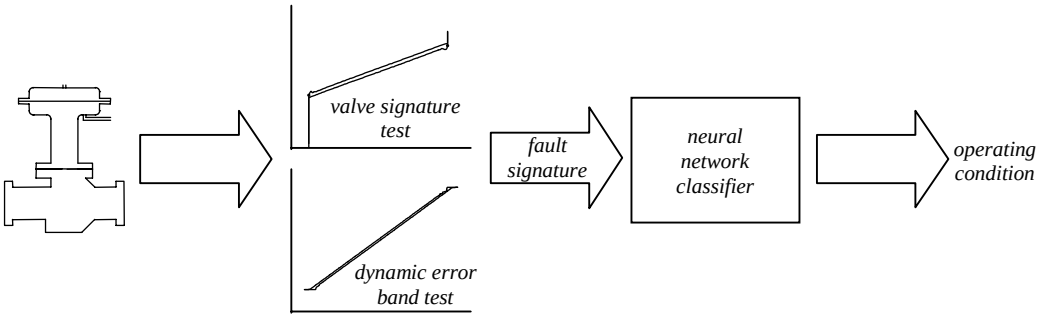

Fig. 8. Fault detection and identification scheme.

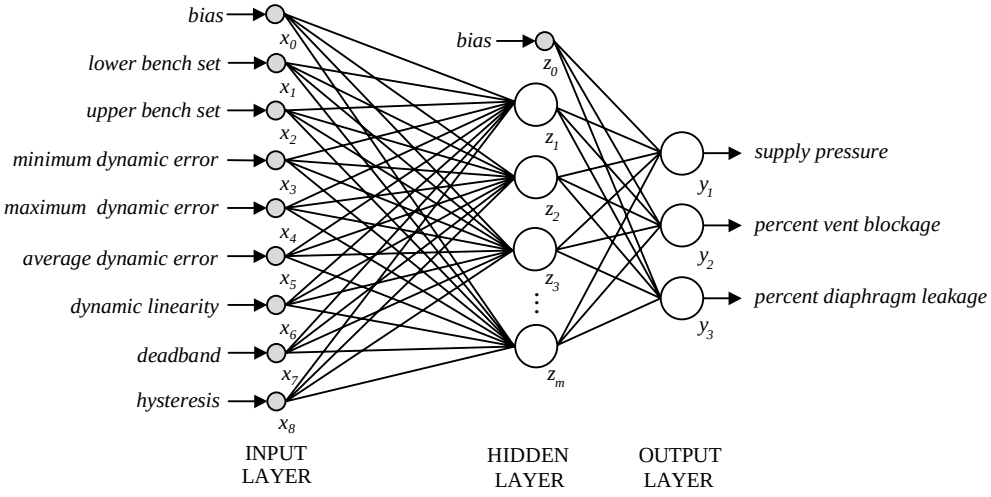

Fig. 9. Network architecture.

indicated when any one of the network outputs deviates from its normal value.

4.1. Network structure

Fig. 9 shows the schematic of the network structure. The network is a multilayer feedforward type consisting of an assemblage of interconnected computational elements, known as neurons (Haykin, 1999) that are arranged into layers. The input layer contains nine nodes, one for each of the eight available performance parameters, and an input to accommodate the bias. Each node in the input layer is connected to all the neurons in the adjacent hidden layer. Similarly, each of the neurons in the hidden layer is connected to all the neurons in the output layer. The number of neurons in the hidden layer is adjustable. Since the network does not contain any feedback loops, its output can be calculated as an explicit function of the network inputs and the network weights. The hidden layer neurons use hyperbolic tangent activation functions. Thus, the outputs of the hidden layer neurons are calculated as

$$z_j = \tanh\left(\sum_{i=0}^{8} w_{ij}x_i\right), \quad j = 1, 2, \ldots, m, \tag{1}$$

where x_i are inputs and z_j are outputs of the hidden layer neurons. The weights, w_{ij}, are the weights between input node i and hidden neuron j. The bias is absorbed into Eq. (1) by taking $x_0 = 1$. The three neurons in the output layer use linear activation functions. The network outputs, y_k, can be written as

$$\begin{aligned} y_k &= \sum_{j=0}^{m} w_{jk}z_j \\ &= \sum_{j=1}^{m} w_{jk}\tanh\left(\sum_{i=0}^{8} w_{ij}x_i\right) \\ &\quad + w_{0k}z_0, \quad k = 1, 2, 3, \end{aligned} \tag{2}$$

where w_{jk} are the weights between neuron j and neuron k in the hidden and output layers, respectively. The hidden layer bias is included in (2) by setting $z_0 = 1$.

4.2. Training data

Twelve faulty operating conditions were examined in this study. They are listed in Table 1, along with the reference (normal) condition. The faulty operating conditions were chosen to reflect a wide range of fault magnitudes within each fault class. Here, all faults are

assumed to occur singly but exist in a multi-fault environment. As such, there are no instances where two or more faults occur simultaneously. Table 2 lists the performance parameters associated with the valve signature and DEB tests obtained experimentally for each operating condition. Table 2 also lists the valve deadband and hysteresis data that were measured manually from the corresponding valve signature plots.

4.3. Network training

The training process establishes the nonlinear mapping between the values of the performance parameters and the corresponding operating condition of the process valve. This is accomplished by adjusting the network weights so that the error between the desired output (the actual operating condition) and the network output (the estimated operating condition) for all sets of training data is minimised. The network was trained to predict the operating conditions listed in Table 1 using the experimentally obtained performance parameters. The adjustable weights were first initialised using the Nguyen–Widrow initialisation algorithm (Nguyen and Widrow, 1990). Since the training data contained both small and large values, they were scaled to lie on the continuous interval $[-1, 1]$. Then, the weights were tuned by error back-propagation using the gradient descent algorithm with momentum. The batch mode of training was used. Thus, the weights were adjusted to minimise the network error over the entire set of training data. Training was terminated when the overall network error fell below 0.001, or the total number of weight corrections (epochs) exceeded 10 000.

To accelerate convergence, the learning rate was adjusted during training using the bold driver technique (Bishop, 1995). The learning rate, η, was adjusted according to

$$\eta_{\text{new}} = \begin{cases} \rho\eta_{\text{old}}, & \Delta E < 0, \\ \sigma\eta_{\text{old}}, & \Delta E > 0, \end{cases} \tag{3}$$

where ΔE is the change in the network error, $E_{\text{new}} - E_{\text{old}}$, resulting from the last weight update. The values of parameters ρ and σ were set to 1.1 and 0.5, respectively (Bishop, 1995). The effect of changing ρ and σ on the speed of learning was not investigated. However, a simulation study was carried out to determine the optimal value of the momentum term. The results showed that setting the momentum term to 0.9 further increased the rate of learning.

Table 1
Listing of normal and faulty operating conditions

Data set	Operating condition	Supply pressure (kPa)	Vent blockage (%)	Diaphragm leakage (%)
1	Normal	124	0	0
2	Incorrect supply pressure fault	110	0	0
3		97	0	0
4		83	0	0
5		69	0	0
6	Diaphragm leakage fault	124	0	10
7		124	0	20
8		124	0	30
9		124	0	40
10	Vent blockage fault	124	50	0
11		124	75	0
12		124	87.5	0
13		124	100	0

Table 2
Performance parameters obtained from valve signature and dynamic error band tests for each operating condition in Table 1

Data set	Lower bench set (kPa)	Upper bench set (kPa)	Minimum dynamic error (%)	Maximum dynamic error (%)	Average dynamic error (%)	Dynamic linearity (%)	Deadband (kPa)	Hysteresis (mm)
1	55.8	111.6	1.48	1.85	1.70	0.11	4.65	1.60
2	55.7	116.6	1.66	2.03	1.89	0.09	4.70	1.60
3	55.6	111.9	2.39	2.90	2.73	0.08	4.51	1.55
4	55.5	112.9	2.19	2.90	2.53	0.13	4.27	1.19
5	55.4	115.1	1.35	2.63	2.07	0.28	2.83	1.32
6	58.5	116.9	1.26	1.87	1.59	0.14	6.23	1.57
7	62.6	127.5	1.86	3.23	2.46	0.26	5.21	1.60
8	67.5	139.3	2.25	3.57	2.86	0.20	7.03	1.85
9	74.1	157.3	2.10	3.35	2.69	0.17	6.62	1.12
10	55.8	111.7	1.46	1.89	1.75	0.10	4.62	1.57
11	55.7	111.8	1.49	1.90	1.76	0.11	4.71	1.55
12	55.7	111.6	2.98	1.89	1.75	0.10	4.84	1.68
13	61.6	170.2	2.63	3.08	2.90	0.08	6.40	1.14

5. Results

Two tests were conducted in order to assess the performance of the networks trained to detect and identify the faulty modes of operation studied here. In the first test, valve deadband and hysteresis data were excluded from the training data sets. This test was motivated by the desire to design a FDI system that would lend itself well to automation. In the second test, all eight of the available performance parameters, including the valve deadband and hysteresis, were used to train the network. The second test served to ascertain whether the addition of the valve hysteresis and deadband as network inputs would improve the overall performance of the network. If the improvements in the network performance are considerable, then the manual extraction of the valve hysteresis and deadband may be well worth the effort.

For each test, the ideal number of neurons in the hidden layer was determined by observing the onset of overfitting. Overfitting of the data was considered to have occurred when the addition of a neuron in the hidden layer did not lead to an increase in the accuracy of the network. One hundred networks were trained for each hidden layer size to minimise the effects of the random assignment of the initial weights. Unless otherwise noted, the results presented here are averaged over the 100 network sets.

Fig. 10 illustrates the unscaled overall network error for both tests, as the number of neurons in the hidden layer is increased from three to 12. This figure illustrates the onset of overfitting in the network since after a threshold number of hidden neurons is reached, no further improvement in the network performance is observed. The overfitting region for the network where the valve deadband and hysteresis were excluded from the training data begins when the number of hidden neurons exceeds six. For the network where all performance parameters were used, the overfitting region begins when there are four neurons in the hidden layer. Thus, a network with 6 hidden neurons is an ideal solution when the deadband and hysteresis are excluded from the training data. Similarly, a network with 4 hidden neurons presents an ideal solution when all of the available performance parameters are used. For the remainder of this paper, the network that does not use the valve deadband and hysteresis as inputs shall be referred to as the reduced data (RD) network. The network that uses all available data as inputs shall be referred to as the full data (FD) network.

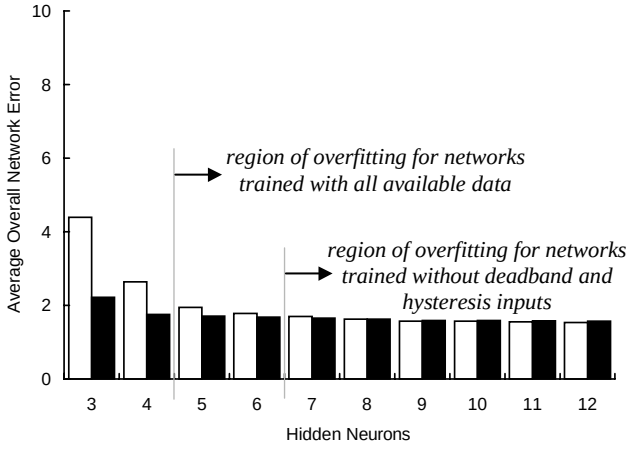

Fig. 10. Average overall network error as the number of neurons in the hidden layer is increased. □, represents networks where valve deadband and hysteresis data are not used. ■, represents networks where valve deadband and hysteresis are included as network inputs.

Tables 3 and 4 list typical outputs of the RD and FD networks when queried with input data corresponding to the faulty operating conditions listed in Table 1. Tables 3a and 4a indicate that the RD and FD networks have learned to both detect and identify the incorrect supply pressure fault. The fault detection is indicated by the variation in the output of the supply pressure neuron, which deviates from its normal value in accordance with the changes in the supply pressure. The networks also possess the ability to differentiate between various magnitudes of the incorrect supply pressure fault. Proper identification of the incorrect supply pressure fault is indicated by the outputs representing the diaphragm leakage and vent blockage, which remain close to their normal values as the supply pressure is varied. Tables 3b, 3c, 4b, and 4c indicate similar results for the diaphragm leakage and vent blockage faults.

Upon inspection of Tables 3 and 4 one observes that the FD network, using all of the available performance parameters, performs similarly to the RD network. This suggests that the addition of the valve deadband and hysteresis may not play a significant role in the overall performance of the network, with the exception of reducing the size of the hidden layer. However, the number of epochs required for the networks to converge can also be considered an indicator of the network performance. With reference to Fig. 11, it is seen that including the valve deadband and hysteresis as network inputs results in a much shorter training time for a given hidden layer size.

To determine where the increase in performance has originated, the network error was assessed for each of the outputs independently. Fig. 12a shows the error in the supply pressure, averaged over all training data sets, for networks with 3–6 hidden neurons. The networks with hidden layer sizes greater than six were excluded as they reside in the overfitting region. For both tests, the error in the predicted supply pressure is seen to decrease as the number of hidden neurons increases. Furthermore, for a given hidden layer size, the networks using the deadband and hysteresis data perform similarly to

Table 3
Outputs of a typical RD network when queried with data representing: (a) incorrect supply pressure fault, (b) diaphragm leakage fault, and (c) vent blockage fault

Data set	Supply pressure (kPa)		Diaphragm leakage (%)		Vent blockage (%)	
	Actual value	Network output	Actual value	Network output	Actual value	Network output
(*a*) *Incorrect supply pressure fault*						
1	124	121.4	0	1.7	0	20.4
2	110	110.0	0	−0.5	0	0.5
3	97	95.7	0	0.5	0	0.8
4	83	83.5	0	−0.2	0	−0.1
5	69	68.8	0	0.0	0	0.1
(*b*) *Diaphragm leakage fault*						
6	124	124.9	10	10.1	0	−1.8
7	124	123.8	20	20.4	0	0.3
8	124	124.7	30	29.6	0	0.0
9	124	124.0	40	40.0	0	−0.4
(*c*) *Vent blockage fault*						
10	124	125.8	0	−0.7	50	51.0
11	124	124.9	0	−1.1	75	53.2
12	124	124.0	0	0.1	87.5	87.1
13	124	124.0	0	0.4	100	99.9

Table 4
Outputs of a typical FD network when queried with data representing: (a) incorrect supply pressure fault, (b) diaphragm leakage fault, and (c) vent blockage fault

Data set	Supply pressure (kPa)		Diaphragm leakage (%)		Vent blockage (%)	
	Actual value	Network output	Actual value	Network output	Actual value	Network output
(*a*) *Incorrect supply pressure fault*						
1	124	119.6	0	0.6	0	1.8
2	110	114.2	0	0.4	0	−1.1
3	97	96.5	0	−0.7	0	0.0
4	83	82.8	0	−1.4	0	−0.1
5	69	70.6	0	−0.3	0	−0.1
(*b*) *Diaphragm leakage fault*						
6	124	124.0	10	10.1	0	0.2
7	124	116.3	20	26.5	0	0.2
8	124	124.2	30	30.8	0	−0.5
9	124	130.2	40	34.1	0	0.3
(*c*) *Vent blockage fault*						
10	124	124.2	0	−0.1	50	50.7
11	124	126.3	0	−0.3	75	73.3
12	124	123.1	0	−0.3	87.5	87.2
13	124	123.4	0	0.6	100	100.7

those that do not. The difference between the two results is much less than 0.7 kPa, and practically insignificant. Fig. 12b shows the error in the network approximation of the diaphragm leakage fault averaged over all training data sets. Again, it is observed that for a given hidden layer size, the improvement in accuracy is negligible when all the available performance parameters are used.

The network error, averaged over the entire training data set, for the vent blockage fault is shown in Fig. 12c. For networks with small hidden layers, it is apparent that the addition of the valve deadband and hysteresis data significantly reduces the network error in the estimation of the degree of vent blockage. It is concluded that the deadband and hysteresis parameters contain discriminatory information that characterises

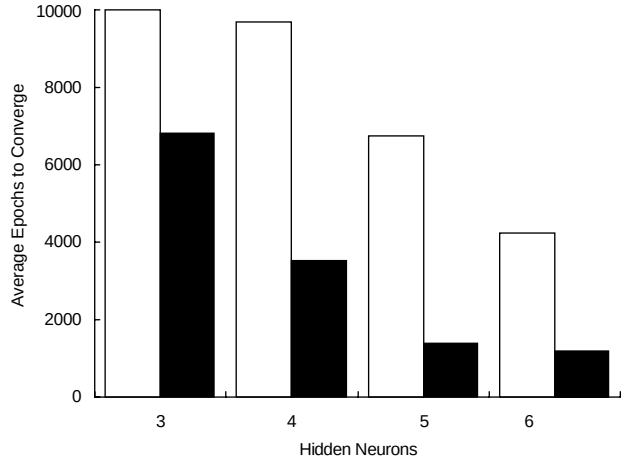

Fig. 11. Average number of epochs to converge as the number of neurons in the hidden layer is increased. □, represents networks where valve deadband and hysteresis data are not used. ■, represents networks where valve deadband and hysteresis are included as network inputs.

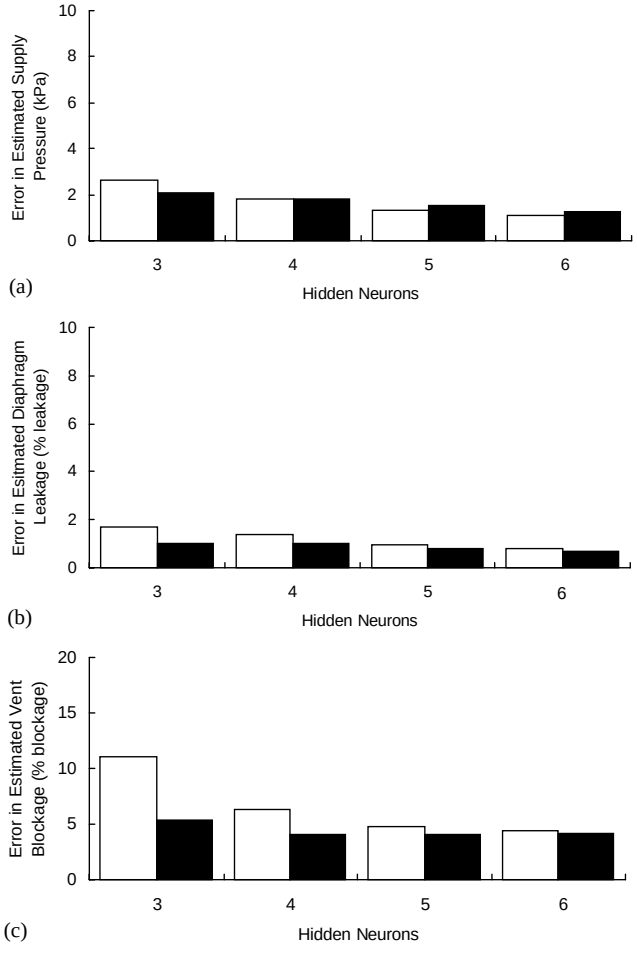

Fig. 12. Average error in the predicted operating condition as the number of neurons in the hidden layer is increased: (a) supply pressure, (b) diaphragm leakage, and (c) vent blockage. □, represents networks where valve deadband and hysteresis data are not used. ■, represents networks where valve deadband and hysteresis are included as network inputs.

the vent blockage fault better than the other performance parameters. Consequently, their inclusion in the training data leads to smaller networks with shorter training times without sacrificing accuracy.

6. Conclusions

A scheme for the detection and identification of actuator faults in a pneumatic control valve, based on a multilayer feedforward neural network, was presented. The network was trained with experimental data obtained directly from a software package that comes with the valve. This eliminated the need for additional instrumentation of the valve. Specifically, the valve signature and dynamic error band tests were used to obtain the lower and upper bench sets, minimum, maximum and average dynamic errors as well as the dynamic linearity. The valve deadband and hysteresis were manually extracted from the available data, and were also used as network inputs.

The test results showed that the trained networks were capable of detecting and identifying incorrect supply pressure, diaphragm leakage, and actuator vent blockage faults of various magnitudes. It was also observed that including the valve deadband and hysteresis as network inputs: (i) enhanced the ability of the network to estimate the vent blockage fault, and (ii) lead to smaller networks with shorter training times.

Having established the methodology, a larger number of data sets together with the cross-validation method of training can now be used to ensure the desensitisation of the network to variations in the performance parameters, for each fault class.

Acknowledgements

The authors would like to acknowledge the assistance of Controltech Inc., Winnipeg, Manitoba, Canada who granted partial funding for this work in addition to providing the control valve used in the research. The authors would also like to extend their deepest thanks to Mr. Larry Mercado (of Controltech Inc.) for generously offering both his time and technical expertise during the course of the project.

References

Bernieri, A., D'Apuzzo, M., Sansone, L., Savastano, M., 1994. A neural network approach for identification and fault diagnosis on dynamic systems. IEEE Transactions on Instrumentation and Measurement 43 (6), 867–873.

Bishop, C.M., 1995. Neural Networks for Pattern Recognition. Oxford University Press Inc., New York.

Borairi, M., Wang, H., 1998. Actuator and sensor fault diagnosis of non-linear dynamic systems via genetic neural networks and adaptive parameter estimation technique. Proceedings of the 1998 IEEE Conference on Control Applications 1, Trieste, Italy, pp. 278–282.

Burrows, C.R., Peckham, R.G., 1977. Dynamic characteristics of a pneumatic flapper valve. Journal of Mechanical Engineering Science 19 (3), 113–121.

Crowther, W.J., Edge, K.A., Burrows, C.R., Atkinson, R.M., Woollons, D.J., 1998. Fault diagnosis of a hydraulic actuator circuit using neural networks — an output vector space classification approach. Journal of Systems and Control Engineering 212 (1), 57–68.

Fisher Controls Inc., 1999a. FIELDVIEW® ValveLink™ VL2000 Series Software User Guide. Fisher Controls International Inc., Iowa.

Fisher Controls Inc., 1999b. Control Valve Handbook. Fisher Controls International Inc., Iowa.

Frank, P.M., 1990. Fault diagnosis in dynamic systems using analytical and knowledge-based redundancy—a survey and some new results. Automatica 26 (3), 459–474.

French, I.G., Cox, C.S., 1990. Modelling, design and control of a modern electropneumatic actuator. Proceedings of the IEE Part D: Control Theory and Applications 137 (3), 145–155.

Haykin, S., 1999. Neural Networks: A Comprehensive Introduction, 2nd Edition. Prentice-Hall, New Jersey.

Isermann, R., 1993. Fault diagnosis of machines via parameter estimation and knowledge processing—tutorial paper. Automatica 29 (4), 815–835.

Isermann, R., 1997. Supervision, fault-detection and fault-diagnosis methods—an introduction. Control Engineering Practice 5 (5), 639–652.

Karpenko, M., Sepehri, N., 2001. A neural network based fault detection and identification scheme for pneumatic process control valves. Proceedings of the 2001 IEEE Systems, Man, and Cybernetics Conference, Tucson, AZ, Vol. 1, pp. 93–98.

Karpenko, M., Sepehri, N., Scuse, D., 2001. Neural network detection and identification of actuator faults in a pneumatic process control valve. Proceedings of the 2001 IEEE International Symposium on Computational Intelligence in Robotics and Automation, Bauff, Canada, pp. 166–171.

Koivo, H.N., 1994. Artificial neural networks in fault diagnosis and control. Control Engineering Practice 2 (1), 89–101.

Le, T.T., Watton, J., Pham, D.T., 1997. An artificial neural network based approach to fault diagnosis and classification of fluid power systems. Journal of Systems and Control Engineering 211 (4), 307–317.

Le, T.T., Watton, J., Pham, D.T., 1998. Fault classification of fluid power systems using a dynamics feature extraction technique and neural networks. Journal of Systems and Control Engineering 212 (2), 87–97.

Leonhardt, S., Ayoubi, M., 1997. Methods of fault diagnosis. Control Engineering Practice 5 (5), 683–692.

Lin, J., Qu, L., 2000. Feature extraction based on morlet wavelet and its application for mechanical fault diagnosis. Journal of Sound and Vibration 234 (1), 135–148.

McGhee, J., Henderson, I.A., Baird, A., 1997. Neural networks applied for the identification and fault diagnosis of process valves and actuators. Measurement: Journal of the International Measurement Confederation 20 (4), 267–275.

Nguyen, D., Widrow, B., 1990. Improving the learning speed of 2-layer neural networks by choosing initial values of the adaptive weights. International Joint Conference on Neural Networks, San Diego, CA, Vol. 3, pp. 21–26.

Sharif, M.A., Grosvenor, R.I., 1998. Fault diagnosis in industrial control valves and actuators. Proceedings of the 1998 IEEE Instrumentation and Measurement Technology Conference, St. Paul, MN, Vol. 2, pp. 770–778.

Sharif, M.A., Grosvenor, R.I., 2000. The development of novel control valve diagnostic software based on the visual basic programming language. Journal of Systems and Control Engineering 214 (2), 99–127.

Sorsa, T., Koivo, H.N., Koivisto, H., 1991. Neural networks in process fault diagnostics. IEEE Transactions on Systems, Man, and Cybernetics 21 (4), 815–825.

Tzafestas, S.G., Dalianis, P.J., 1994. Fault diagnosis in complex systems using artificial neural networks. Proceedings of the I EEE Conference on Control Applications 2, Glasgow, UK, 877–882.

Yen, G.G., Lin, K., 2000. Wavelet packet feature extraction for vibration monitoring. IEEE Transactions on Industrial Electronics 47 (3), 650–667.

Zhang, J., Ma, J., Yan, Y., 2000. Assessing blockage of the sensing line in a differential-pressure flow sensor by using the wavelet transform of its output. Measurement Science and Technology 11 (3), 178–184.